(12)

NSWCDD/TR-93/138

NUMERICAL SIMULATION OF LATERAL THRUSTERS IN HYPERSONIC FLOW OVER A BICONIC BODY

BY T. HSIEH AND A. B. WARDLAW, JR.

SYSTEMS RESEARCH AND TECHNOLOGY DEPARTMENT

8 MARCH 1994

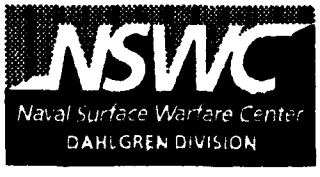

NAVAL SURFACE WARFARE CENTER
DAHLGREN DIVISION • WHITE OAK DETACHMENT
Silver Spring, Maryland 20903-5640

NSWCDD/TR-93/138

NUMERICAL SIMULATION OF LATERAL THRUSTERS IN HYPERSONIC FLOW OVER A BICONIC BODY

BY T. HSIEH AND A. B. WARDLAW, JR.
SYSTEMS RESEARCH AND TECHNOLOGY DEPARTMENT

8 MARCH 1994

NAVAL SURFACE WARFARE CENTER
DAHLGREN DIVISION • WHITE OAK DETACHMENT
Silver Spring, Maryland 20903-5640

FOREWORD

The lateral thrusters and the shock layer on the THAAD missile are studied through numerical simulation using a Navier-Stokes code. This report describes the simulation, presents the computed flow field and indicates the conditions under which jet flow is trapped upstream of the jet.

This report was sponsored by the Naval Surface Warfare Center, Dahlgren Division, ATBM Program Office under the direction of Pete Stafford. The aerothermal group coordinator was Frank Moore.

Approved by:

George Long

GEORGE LONG
Head, Missile Program Office

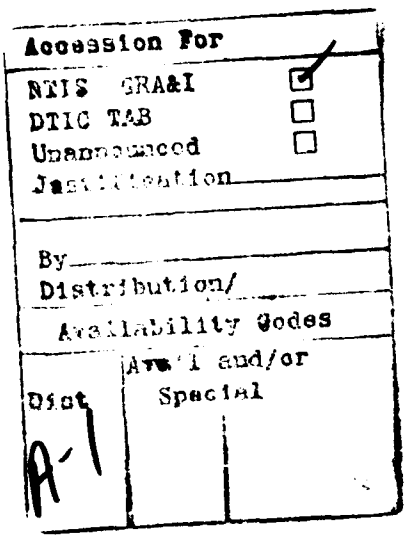

ABSTRACT

A Navier-Stokes simulation of lateral thrusters on a biconic body in hypersonic flow is presented. Due to simplifications arising from symmetry, cruciform thrusters were considered first. A grid convergence was conducted to evaluate computational accuracy. This was followed by the computation of three different jet exit conditions and an assessment of the flow field changes produced by each. Of particular concern was the possibility of entrapment of streamlines from the jet in a recirculation region upstream of the jet. The final case considered was a single jet thrusting from a biconic body at zero incidence at M = 9.7. These results were compared to experimental surface pressures. A description of the complicated interacting flow fields featuring multiple separation and attachment lines/regions is also presented.

CONTENTS

ILLUSTRATIONS

TABLE

CHAPTER 1

INTRODUCTION

The interaction of a lateral thruster and the surrounding flow field falls into the the category of jet interaction. This topic has also been the subject of research for decades in connection with combustion mixing[1] and more recently in conjunction with high speed aerodynamics control.[2–10] The typical jet interaction flow field is complex; it is characterized by shock/shock interactions, shock/boundary layer interactions, three-dimensional turbulent mixing, high temperature combustion and large regions of flow separation. The separation regions may contain numerous vortices which interact in an inherently unsteady manner. Currently, limited information is available concerning this type of flow field. This is a result, at least in part, of the difficulty in providing sufficient instrumentation to measure such a flow field and the expense of wind tunnel testing. Accordingly, a sufficient jet interaction data base is not currently available to support engineering design.

Recent reports describing the use of Navier-Stokes models for solving the equations with turbulence and chemistry models[4–11] show encouraging results in predicting the jet interaction flow field. However, there are notable discrepancies between calculation and experiment. Measurements in Reference 6 indicate that the presence of the relatively small jet causes a pressure rise on the opposite side of the body. The numerical simulation reported here failed to predict this pressure rise. Later, in Reference 9, McDonough et al. using the same Navier-Stokes solver, computed such a pressure rise to some extent, but did not achieve a final solution.

The purpose of the present work is threefold: (1) to predict the aero/fluid-dynamics of a hypersonic biconic body with lateral thrusters, (2) to assess the accuracy of the numerical simulation by comparing the computation with experiments and (3) to predict the features of the jet induced circulation region; its extent and to assess the possibility of jets streamline entrainment. These goals are accomplished with the Navier-Stokes solver (CFL3D), which initially is applied to an axisymmetric vehicle with four jet located in a cruciform arrangement. The symmetry exhibited by this configuration reduces the computational requirements and facilites a mesh convergence study. This is followed by an examination of the influence of different jet conditions on the flow field. Finally, the CFL3D code is applied to the single jet problem of Reference 6. The study is concluded by examining the details of the separation region.

CHAPTER 2

NUMERICAL PROCEDURES

The flow is assumed to be a nonreacting, perfect gas (air) and the boundary layer is taken to be laminar. The Navier-Stokes (N-S) solver used in this study is the CFL3D[12–13] code. The governing equations are the single/double thin layer approximations to the three-dimensional, time-dependent, compressible N-S equations, written in generalized coordinates (ξ, η, ζ) and conservation form as follows:

$$\frac{\partial}{\partial t}(Q) + \frac{\partial}{\partial \xi}(F) + \frac{\partial}{\partial \eta}\left(G - G_v\right) + \frac{\partial}{\partial \zeta}\left(H - H_v\right) = 0 \tag{1}$$

where $Q=(J^{-1})(\rho, \rho u, \rho v, \rho w, e)^T$, F, G, H are the inviscid flux vectors and the subscript v stands for the corresponding viscous flux vectors (see Reference 12 for G_v and H_v), $J=\partial(\xi,\eta,\zeta)/\partial(x,y,z)$, ρ is the density, e is the total energy, and u,v,w are the x,y,z Cartesian velocity components. The equation of state for an ideal gas is used to define the pressure $p=(\gamma-1)[e-\rho(u^2+v^2+w^2)/2]$, where γ is the ratio of specific heats. Stokes hypothesis for bulk viscosity and Sutherland's law for molecular viscosity are used to close the system.

The flux difference splitting scheme of Roe [14] is chosen for all the generalized fluxes F, G, and H. For example, the flux difference in the ξ–direction at the ith cell for F is split into forward and backward contributions,

$$(\partial F/\partial \xi)_i = F_{i+\frac{1}{2}} - F_{i-\frac{1}{2}} \tag{2}$$

$$F_{i+\frac{1}{2}} = \left[F(q^-) + F(q^+) - |\tilde{A}|\left(Q^+ - Q^-\right)_{i+\frac{1}{2}}\right] \tag{3}$$

where $q^{\pm}$ denotes state variables on cell interfaces and $\tilde{A} = \partial F/\partial Q$ is the averaged value at cell interface. Definition for other symbols in Equations (3) may be found in Reference 12. The diffusion terms are treated using a central difference. The linearized, backward-time approximation in delta form is used for the time differencing. When treated with the spatially factored scheme, the three dimensional equations are solved by a series of sweeps through the three directions as follows:

$$\left[\frac{I}{J\Delta t} + \delta_\zeta\left(\frac{\partial H}{\partial Q} - \frac{\partial H_v}{\partial Q}\right)\right]\Delta Q^* = -L\left(Q^n\right) \tag{4}$$

$$\left[\frac{I}{J\Delta t} + \delta_\eta\left(\frac{\partial G}{\partial Q} - \frac{\partial G_v}{\partial Q}\right)\right]\Delta Q^{**} = \left(\frac{I}{J\Delta t}\right)\Delta Q^* \tag{5}$$

$$\left[\frac{I}{J\Delta t} + \delta_\xi\left(\frac{\partial F}{\partial Q}\right)\right]\Delta Q = \frac{I}{J\Delta t}\Delta Q^{**} \tag{6}$$

$$Q^{n+1} = Q^n + \Delta Q \tag{7}$$

where $-L(Q^n)$ is the discrete representation of the spatial derivative terms in Equation (1) evaluated at time level n. The algorithm is written in delta form so that the steady-state solution is independent of the time step Δt. The implicit spatial derivatives for the convective and pressure terms are first order accurate. This leads to a block tridiagonal solution. Second order accurate upwind-biased spatial differencing is maintained for the residual calculation producing a second order steady state solution. Successful experiences in the application of CFL3D code to the prediction of the flow field about a body of revolution at high incidence in supersonic speed have been reported.[15]

CHAPTER 3

CONVERGENCE OF SOLUTION

The following biconic model was picked for these tests:

forecone half-angle of 15°
aftcone half-angle of 2.1°
diameter at the biconic juncture of 23.5 cm
base diameter of 30. cm
nose radius of 2.2 cm
total length of 1.264 m

Figure 1 provides the biconic body and the grid in the meridian plane. The three-dimensional grid was obtained by rotating the 2D-grid with respect to the body axis. In order to facilitate numerical modeling, a fully symmetric problem of four equally spaced jets was simulated, which reduced the problem to a quarter of the flow field/body. Actually only one eighth of the flow field/body was needed for the fully symmetry problem. However, to facilitate computations of a two-jet case, the quarter model was chosen.

Boundary conditions are explicitly implemented. On the body surface, no-slip, no-penetration, and isothermal wall conditions are imposed. For the singular axis, a continuation of cell center flow variables is imposed. At the far-field inflow boundary, the free-stream condition holds. At the outflow plane, an extrapolation of flow quantities is implemented. The flow is assumed to be symmetrical with respect to the pitching and yawing planes where the jets are located, so only a quarter of the crossflow plane needs to be computed.

The computer program was modified to treat the jet interaction problem by changing the body boundary condition to allow inflow at the jet location. The inflow jet properties are characterized by specifying constant velocity, density, and pressure over the jet exit area. Computation for the body without the jets in operation was carried out first with the initial conditions of uniform free stream everywhere except at solid boundaries where $u = v = w = 0$ was applied. The calculation was continued with the jets turn on and terminated when a converged solution was obtained.

A grid convergence study was carried out for Jet III of Table 1 at a free stream Mach number of 6.5. The jet exit was a 5.1 cm square extending from x = 0.511 m to 0.562 m. The grid sequence consisted of the following meshes: 65x25x49, 97x37x73 and 129x49x97. Here the three dimensions refer to the axial, circumferential and radial directions respectively. The finest mesh, grid III, is illustrated in Figure 1. Figure 2a and 2b show the surface pressure coefficient, Cp, along the meridian plane at the circumferential angles of $\beta = 0°$ and 45° for all three grids. Here the $\beta = 45°$ plane coincides with the symmetry plane for the

computation domain. Good convergence characteristics are achieved for x< 0.38m and x> 0.84m. The remaining region includes the recirculation region in front of the jet and the reattachment region. Discrepancies between the results achieved on the different meshes are visible, particularly for Grid I. These results indicate that a fine grid is needed to resolve the flow in the recirculation region. It appears desirable to used at least the mesh density of Grid II in this region. The computational results also indicated that the flow in the recirculation region may be unsteady, but the fluctuating quantities appear to be relatively small.

CHAPTER 4

THE INFLUENCE OF THE JET PARAMETERS ON THE SHOCK LAYER

Calculations were completed on a 97x37x49 mesh for the three different jets shown in Table 1. The exit conditions for jets I and II were derived assuming a fixed thrust. Jet I satisfied this constraint with a high exit pressure, high exit density and low exit velocity while jet II employed a high exit velocity, low exit density and low exit pressure. Jet III was obtained by arbitrarily varying the density and pressure of Jet II.

The solutions for jets I, II and III illustrate the influence of jet exit conditions on shock layer flow field structures. Of particular interest is entrapment of the jet streamlines in the recirculating zone ahead of the jet. Particulates in the jet exhaust may then be deposited on the body surface. If an antenna window is located beneath the recirculation window, these deposits may obscure the window and impair its operation. Traces of streamlines in the jet-shock layer flow field are shown in Figures 3a, 3b, 3c, where the red streamlines originate from the jet and the blue lines in the free stream. These streamline traces demonstrated that in the case of jet I with the lower jet exit velocity and higher jet exit pressure, streamlines originating from the jet were trapped in the recirculation region ahead of the jet and that the recirculation region extended all the way to the biconic cone juncture. Such entrapment did not occur for jets II and III which featured the higher jet exit velocity and lower jet exit pressure. Also jet III displaced the shock farther from the body than jet II. Thus in general it appears that increasing the jet exit density and pressure disrupts the flow field to a greater extent.

CHAPTER 5

SINGLE JET

COMPARISON WITH EXPERIMENT

Further assessment of the numerical simulation was conducted by comparing calculations and experiments in the case of a body with a single jet. Here the the model was a biconic with a forecone half-angle of 10.4° and aftcone half-angle of 6°. The base diameter, biconic juncture diameter and nose radius were 21cm , 10.4 cm, and .84 cm respectively. This configuration was tested at a free stream Mach number of 9.7 and angle of attack of zero degrees. Surface pressure measurements were taken over the entire body.[6,9] The jet was located at the upper symmetry plane, circumferential angle β = 0°, and axial station of x = 0.417 m. The jet nozzle was oriented normal to the model centerline and had a throat diameter of 1 cm., exit diameter of 1.42 cm (measured normal to the nozzle center line where it intersects the vehicle surface), and a divergent conical section with a half–angle of 15°. The test conditions are:

Free stream Mach number = 9.7
Free stream dynamic pressure = 5.05 lb/in^2
Free stream static pressure = 0.076 lb/in^2
Free stream static temperature = 110° R
Jet stagnation pressure = 155 lb/in^2
Jet stagnation temperature = 540° R

The resulting Reynolds number is 3 x 10^6/ft. The free-stream and the jet gasses were nitrogen, γ = 1.4, while the majority of the boundary layer was laminar.[16]

The jet exit conditions were obtained from a one-dimensional nozzle analysis based on a total pressure and temperature of: ρ_j/ρ_{inf} = 72.7, U_j/U_{inf} = 0.358 (M_j = 2.2), and p_j/p_{inf} = 181. Figure 4 shows the meridian plane of the mesh used in the numerical simulation which consisted of 129x49x97 grid points. In the circumferential direction, the jet was covered by six equal width cells with a span of slightly less than 1°. Progressing circumferentially towards the opposite side of the model, the circumferential spacing was gradually increased to a maximum 5.62°. However, grid points were constrained to coincide with the location at which experimental data was taken in order to facilitate comparison between numerical solution and experiment. The circular jet was approximated in a stair-step fashion by the rectangular surface mesh used in the computation as shown in Figure 5 with a resulting error in area of less than 1 percent.

The comparison between the calculated and measured surface pressure without the jet is shown in Figure 6. Good agreement is obtained with a maximum difference of less than 10 percent. Similar comparisons with the jet on are provided in Figures 7a to 7h for β = 0°, 22.5°, 45°, 62.5°, 90°, 112.5°, 135°, and 180°, respectively. The general trend of the measured pressure distribution from β = 0° to 180° is well predicteded by the numerical solution. Of particular interest is the measured pressure rise at β = 180° and x = 0.4 which is well predicted. This pressure rise is caused by a local thickening of boundary layer which is a result of flow separation induced by jet which is located on the opposite side of the model.

FLOW STRUCTURE

Select body surface and the flow field streamlines are shown in Figures 8 and 9. In Figure 8, the jet streamlines (red) both on and off the symmetry plane escape entrapment in the separation region ahead of the jet. A few jet streamlines move laterally, but most remain part of a cohesive stream which is washed down stream. Figure 8 clearly shows the separation lines (convergence of surface streamlines) and attachment lines (divergence of surface streamlines) on the body surface. This is also illustrated in Figures 9a and 9b which provides views of the body from two different roll orientations. Here jet streamline traces are limited to the pitch plane and the recirculation region can be seen to extend upstream of the jet by about seven jet diameters (see Figure 9a). In Figure 9b, there is an increase of the boundary layer thickness at the location where the first separation line approaches the symmetry plane, but a flow reversal is not evident here. The location of the surface pressure rise shown in plot of Figure 7h matches this point at which the boundary layer thickens.

The lateral jet interactive flow field is analyzed using a topological description which is constructed from streamline traces. The definitive features in this type of model are nodes and saddle singularities, as is described in Reference 17. A topological diagram of the surface and jet side pitch plane is given in Figure 10 which indicates the four separation lines, SL_1 to SL_4 and two attachment lines AL_1 and AL_2. An enlargement of the region containing the jet and its associated recirculation region is shown in Figure 11. This figure includes labels for the singular points and the streamlines originating upstream of this region. Here N designates a node, S a saddle, and the subscripts a and s are fixed to surface singularities to denote attachment or separation. In Figure 11, the oncoming flow is divided into 6 layers, which are separated by the lines labeled 1 to 6 . Layer 6 extends outward from line 6, layer 5 is enclosed by lines 5 and 6 and in general layer n in enclosed by lines n and n+1. From Figure 11 it is evident that layer 6 includes fluid which passes outside of the jet and recirculation region. The fluid contained in layer 5 goes into spiral node N_1 while that in layers 4 and 2 goes into the spiral node N_2. Similarly, the fluid in layer 3 goes into the spiral node N_3 and that in layer 1 ends up at the saddle attachment point Sa_1. Saddle points are located between the nodal pairs of (N_1, N_2), (N_3, N_2), and (N_2, Sa_1). The nodal point N_4 which is located upstream of the jet and very near the surface, feeds both the nodal attachment points Na_1 and Na_2 and the saddle attachment point Sa_2 . Just in front of the jet, there is a saddle separation point Ss_1 on the body surface. Behind the jet, the flow structure is much simpler. Nodal

point N_5, which is similar in type to N_4 and exhibits only outwards flowing streamlines, feeds body surface point Na_3. An additional separation node, Ns_1, is located right behind the jet.

Detail streamline traces do not reveal horseshoe vortices around the jet. The vortices N_1, N_2, and N_3 only remain intact for a distance of about one jet radius away from the symmetry plane and then quickly break apart. A color contour plot of the Mach number distribution in the symmetry plane is shown in Figure 12. The bow shock created by the body and the jet compares well with the Schlieren photograph given in Reference 6. The thickness of the shock layer on the jet side of the body, at the base of the model, is about 3.5 times that on the opposite side of the body. Low Mach number regions can be identified by the dark blue color and they occur near the boundary layer, the recirculation region and behind the jet.

LIFT AUGMENTATION

The lift augmentation due to lateral jets is important in engineering applications. In wind tunnel testing, the augmented lift is computed[18] as follows:

(Lift augmentation) = (jet on, flow on lift)– (jet off, flow on lift)– (jet on, flow off lift)

In numerical simulation, the corresponding lift augmentation is defined,

(Lift augmentation) = (jet on, flow on lift)– (jet off, flow on)

The (jet on, flow off lift) is not necessary in the simulated results since the computed lift is obtained by integrating the surface pressure, without including the jet thrust. Normally the lift augmentation is small at zero incidence and become significant as incidence increases.[18] In this report, only zero incidence was investigated and the jet exit was relatively small, the lift augmentation was small, about 1.5 percent of the jet thrust.

CHAPTER 6

SUMMARY AND CONCLUSIONS

A Navier-Stokes simulation of lateral thrusters on a biconic body in laminar, hypersonic flow is presented. The thruster is characterized by specifying a constant velocity, density, and pressure over the jet exit area. The computed flow field contains the appropriate features including a recirculation region in front of the jet. Three points were considered in detail by the study: the influence of mesh size, the effect of varying the jet properties and a detailed comparison of calculation and experiment.

A grid convergence study was performed for a configuration with four cruciform thrusters located on a biconic body at zero incidence and M = 6.5. A detailed comparison of surface pressures indicates good convergence properties except in the vicinity of the recirculation region. Here a very fine mesh is necessary to capture the vortical and shock structures which occur.

Three jets with different exit velocities, densities and pressures have been studied and results can be summarized as follows: (1) for a given thrust, the jet with the lower velocity and higher pressure penetrates the farthest into the shock layer; (2) jet streamlines may be trapped in the jet created upstream recirculation zone; and (3) increasing the density and pressure of the jet will increase the jet penetration.

Comparison with experiment was carried out by considering a single lateral jet on a biconic body at M = 9.7 and zero incidence. Good agreement was obtained between the measured and calculated surface pressure. This includes correctly predicting a pressure rise on the side of the body opposite to the jet which had been missed or partially missed by others.[6,9] For this case, jet streamline entrapment in the recirculation region did not occur. However, the computed separation region extended seven diameters upstream of the jet. On body surface, four separation lines and two attachment lines could be identified. The computed flow field was also analyzed from the topological point of view by constructing singular points from the streamline patterns. In the jet side of the pitch plane numerous saddle points and nodal points were detected, including a saddle attachment type point which has recently been identified in Reference 19.

This study has laid the ground work for the use of Navier-Stokes solvers in predicting lateral thrust preformance. The current work provides proof of principle for the use of such techniques in the analysis of wind tunnel models where the jet and ambient gasses are of the same type. Extension to the case of different jet-ambient gasses appears be be easily within reach. However, computations for a jet with reacting products represents a more formidable task.

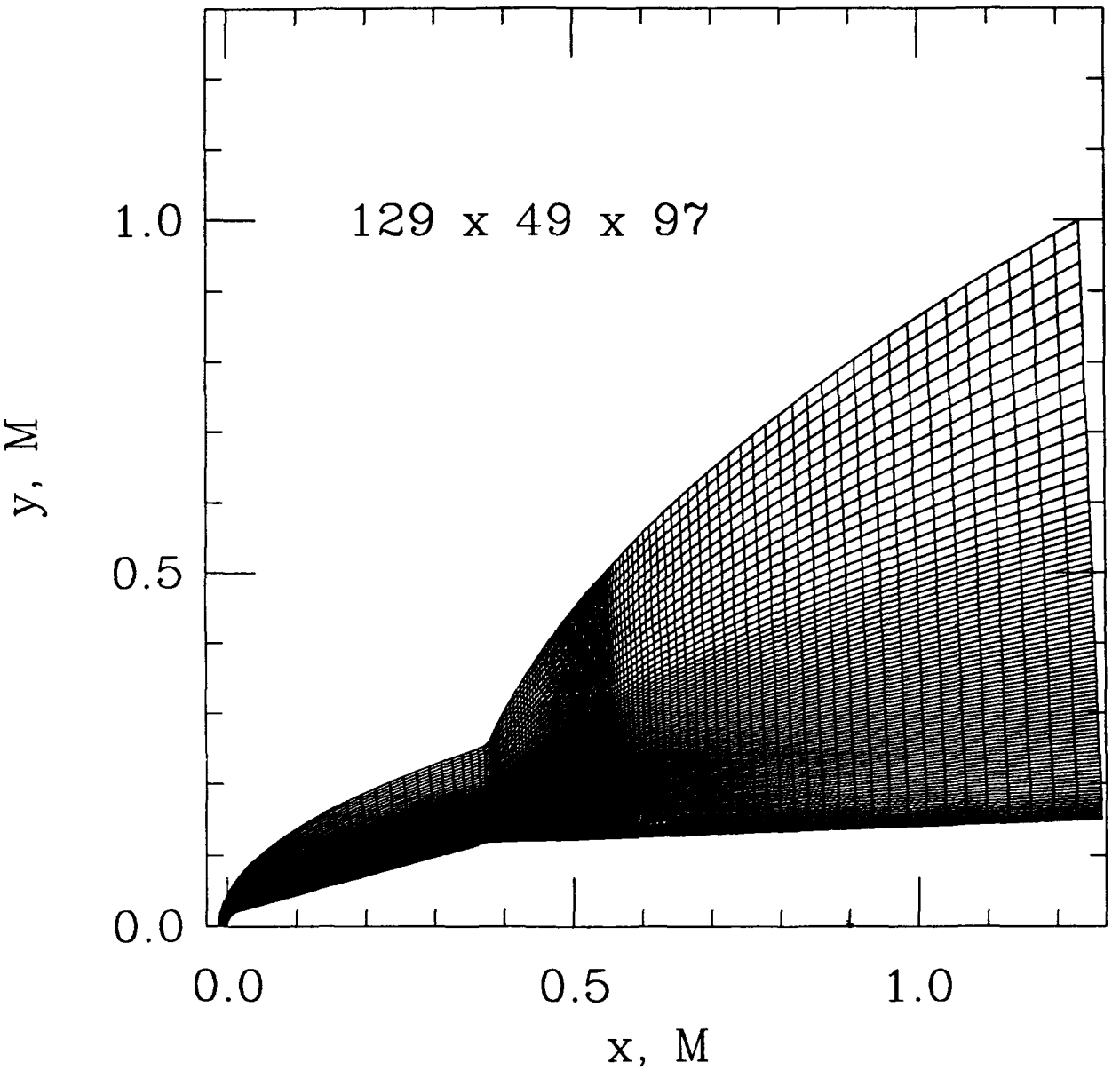

FIGURE 1. COMPUTATIONAL DOMAIN AND GRIDS FOR SYMMETRIC JETS

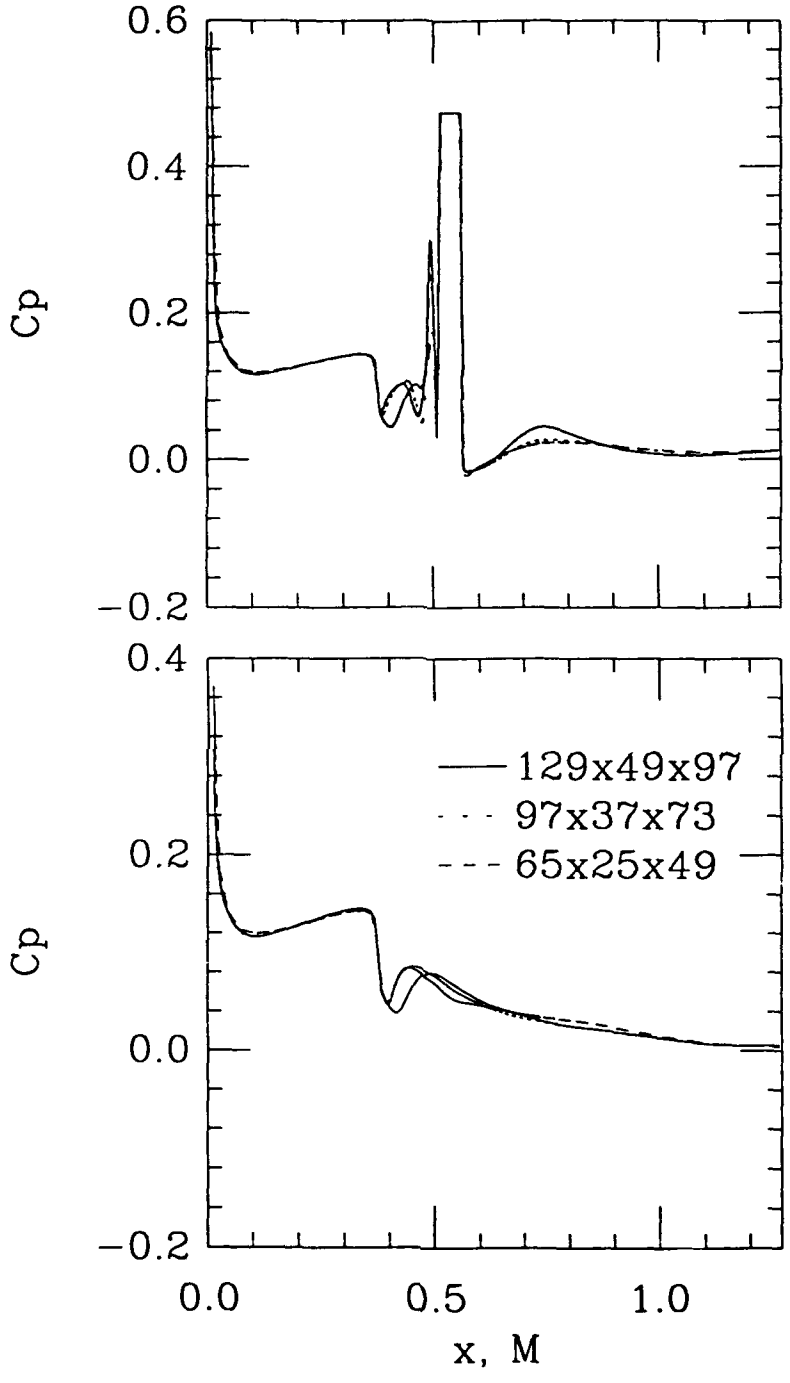

FIGURE 2. COMPARISON OF SURFACE PRESSURE USING THREE GRIDS

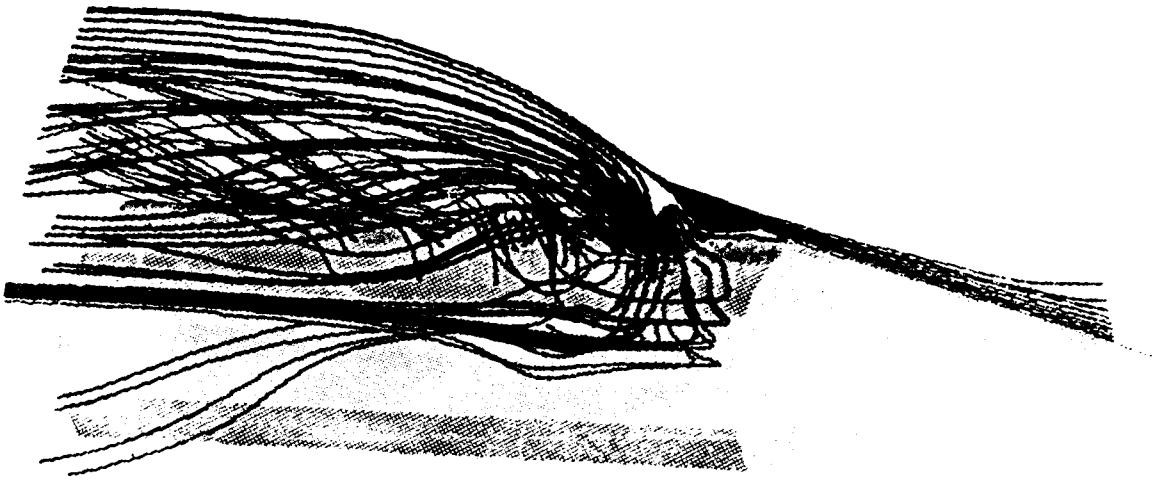

Jet I

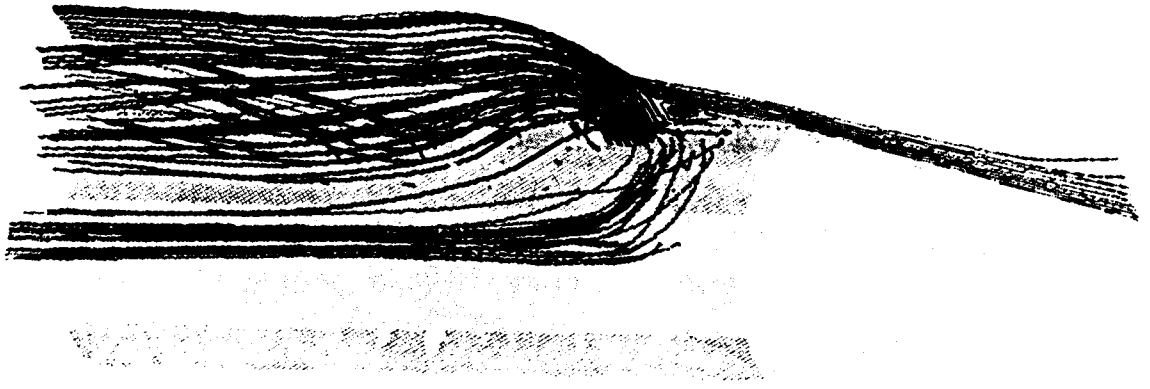

Jet II

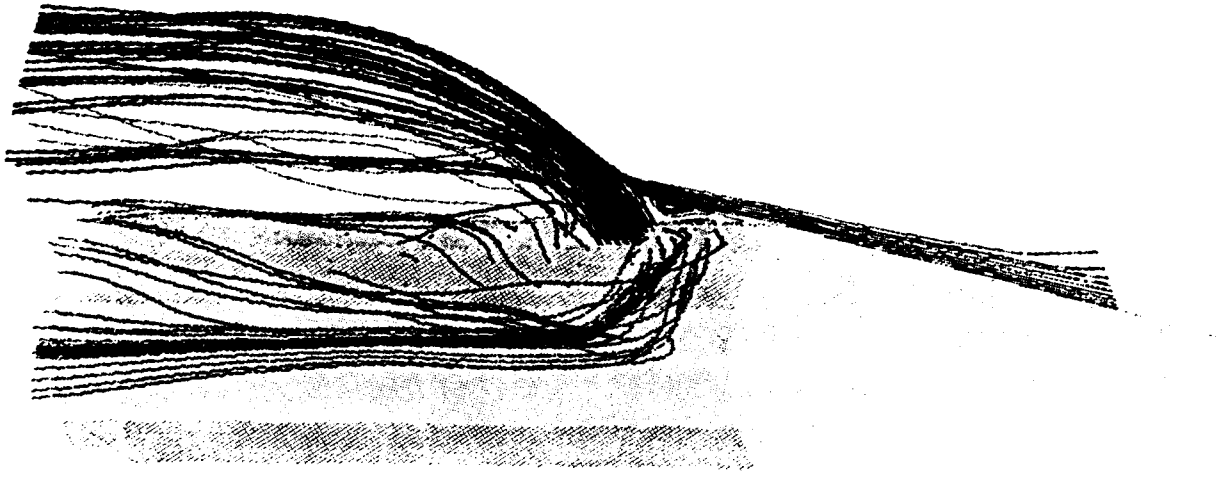

Jet III

FIGURE 3. THREE DIMENSIONAL STREAMINES FOR JETS I, II AND III.

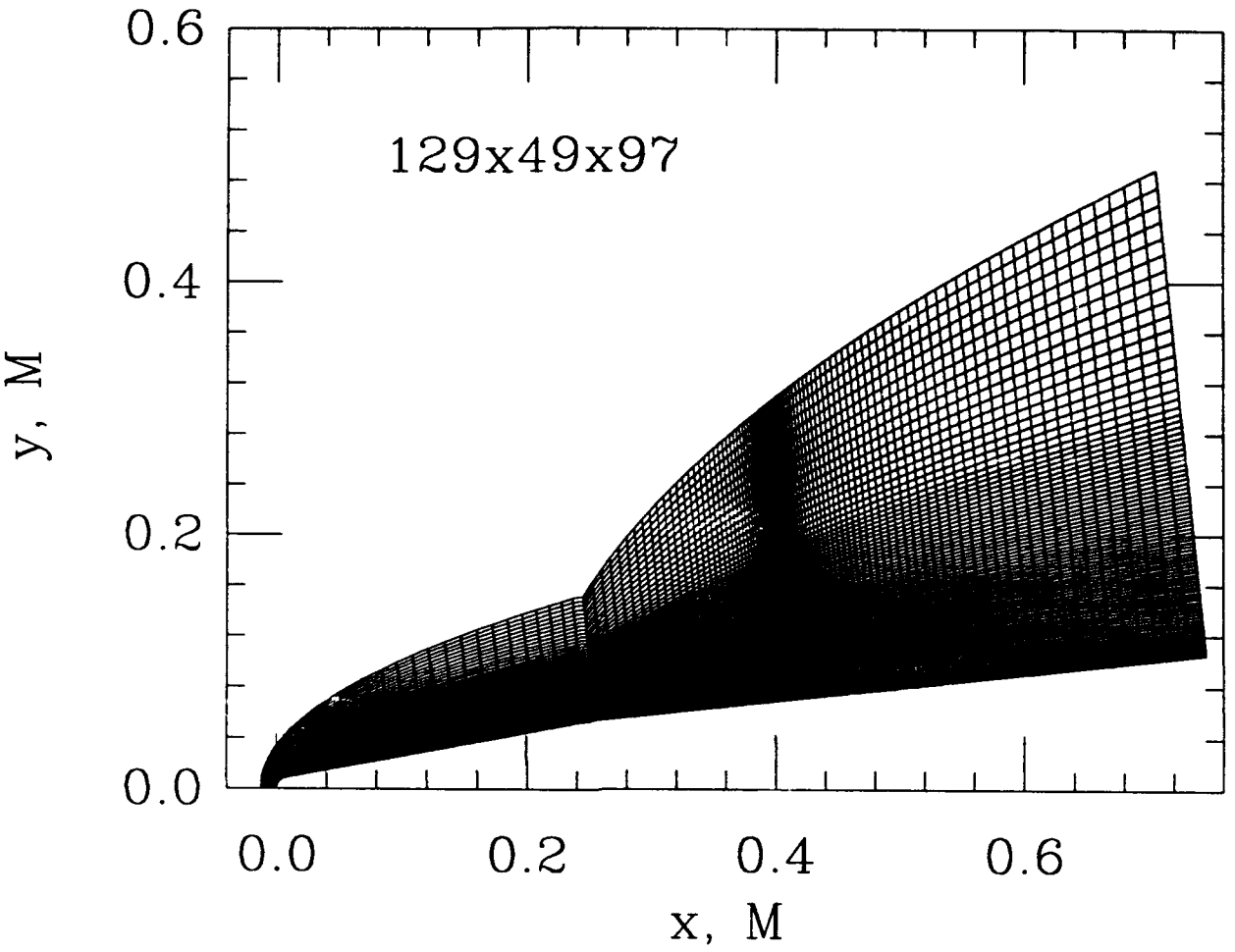

FIGURE 4. COMPUTATIONAL DOMAIN AND GRID FOR SINGLE JET

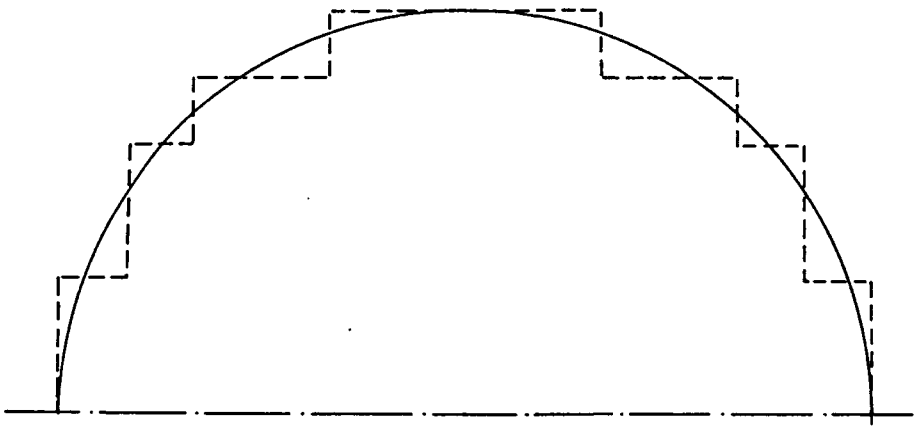

FIGURE 5. APPROXIMATION FOR ROUND JET EXIT GEOMETRY

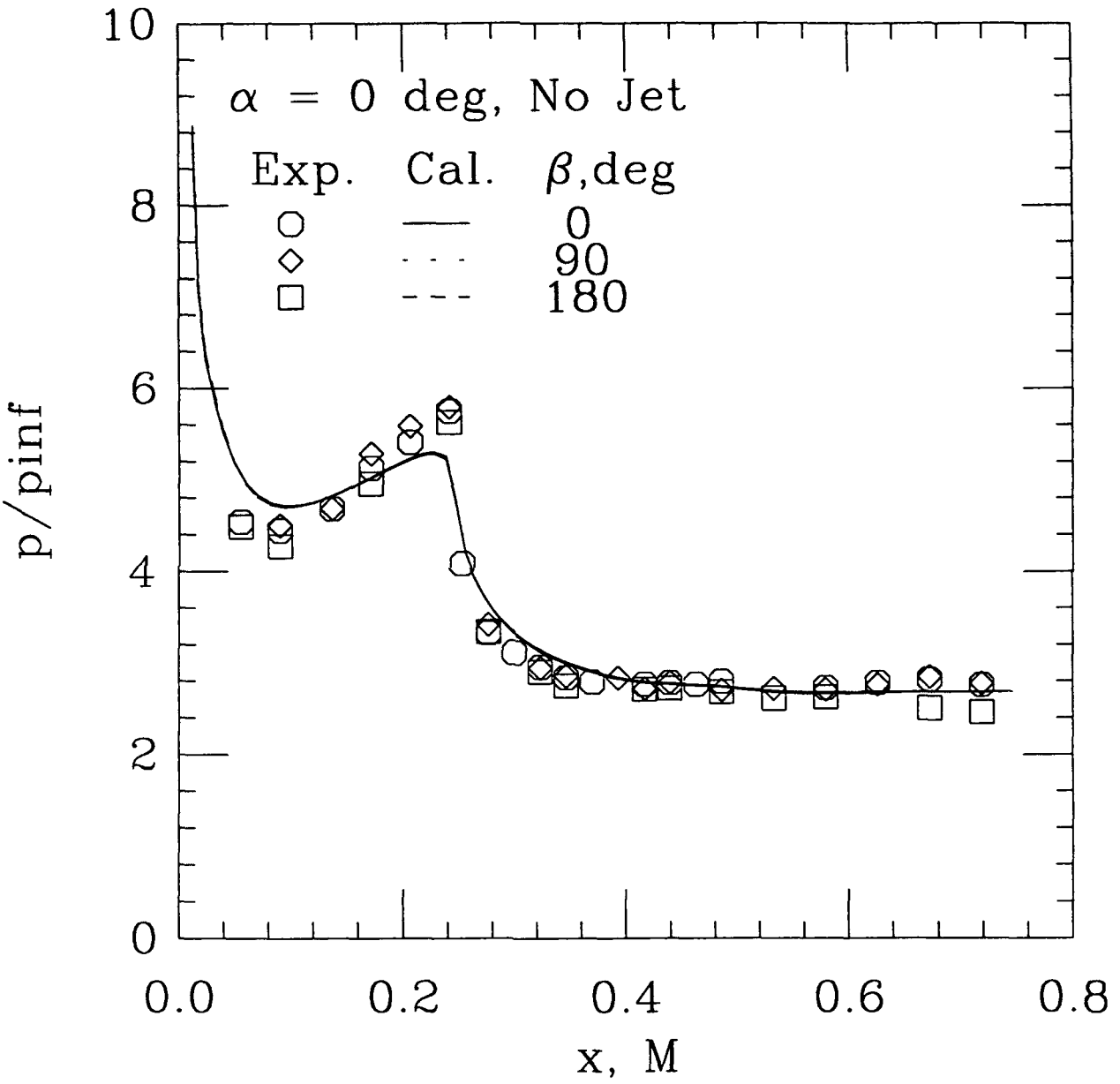

FIGURE 6. COMPARISON OF SURFACE PRESSURE WITHOUT JET

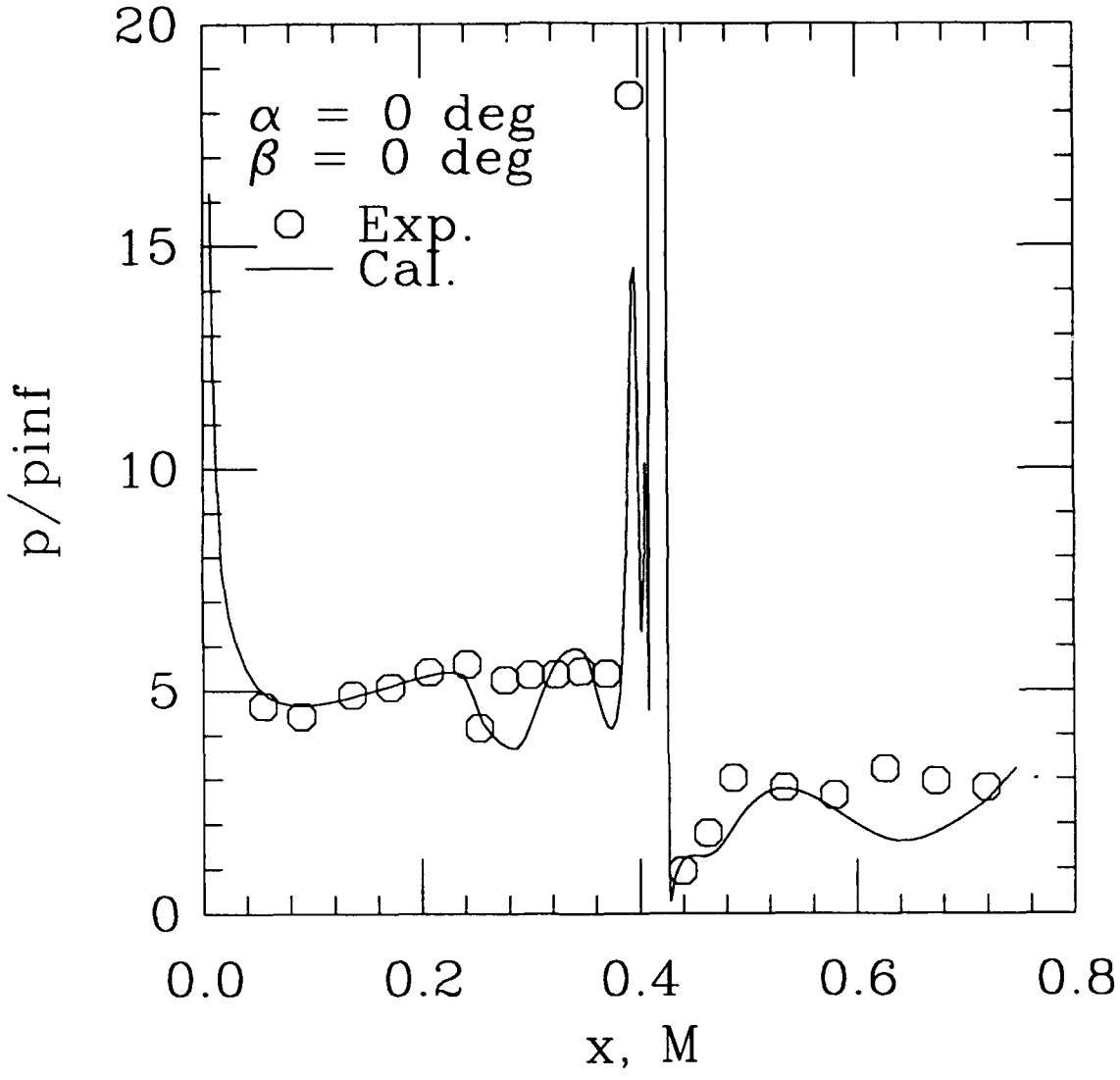

(a)

FIGURE 7. COMPARISON OF SURFACE PRESSURE WITH JET

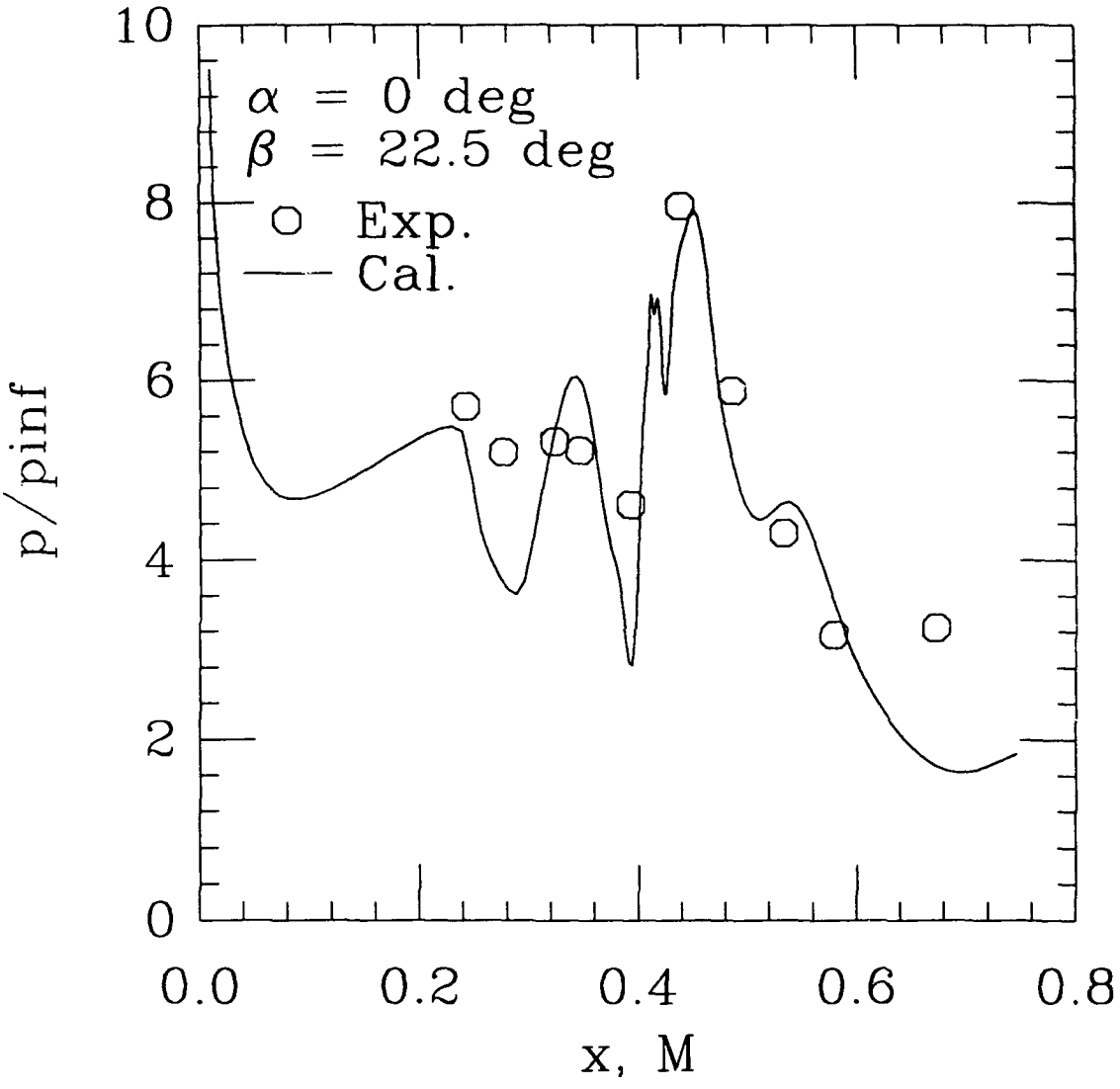

(b)

FIGURE 7. CONTINUED

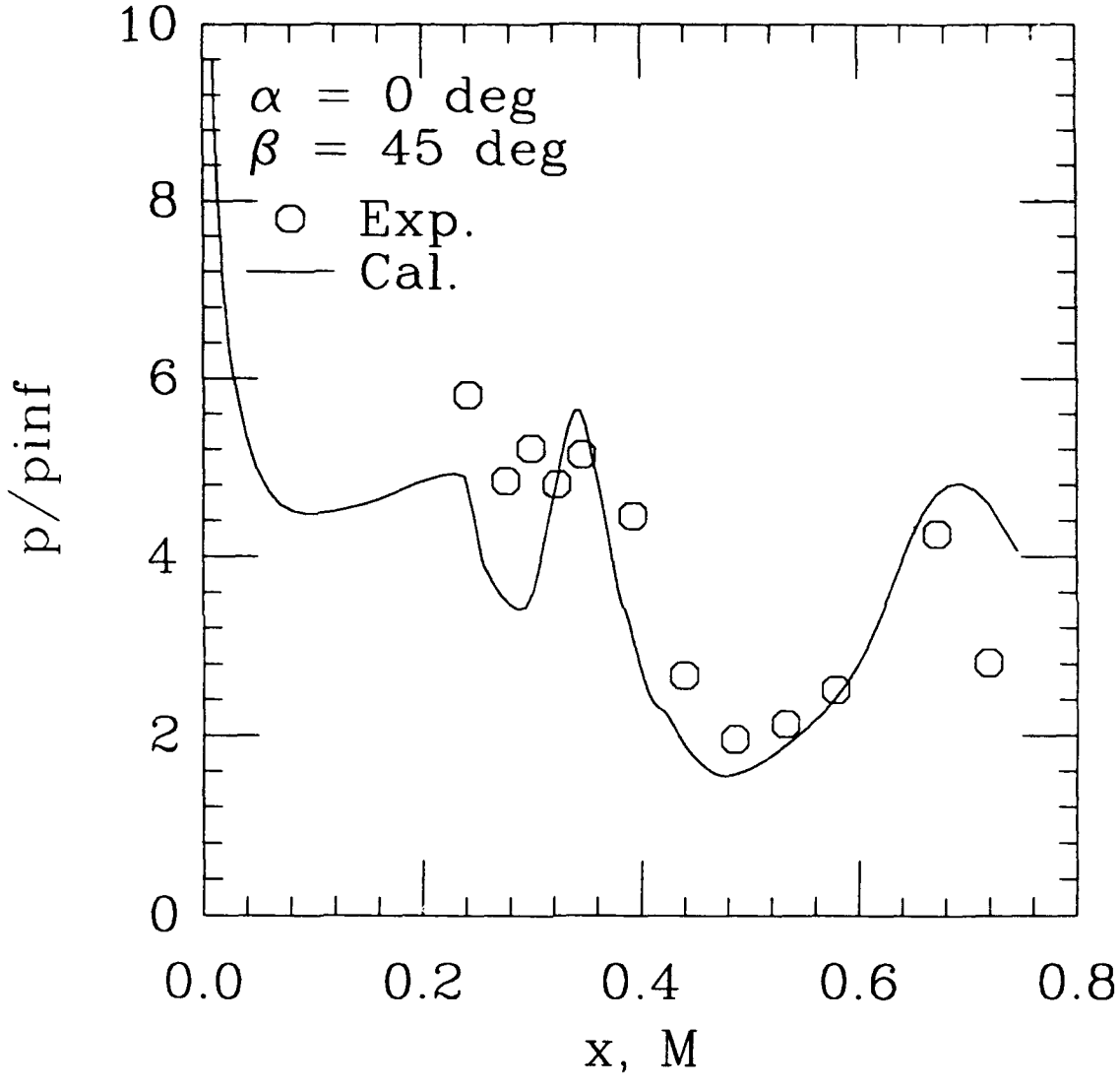

(c)

FIGURE 7. CONTINUED

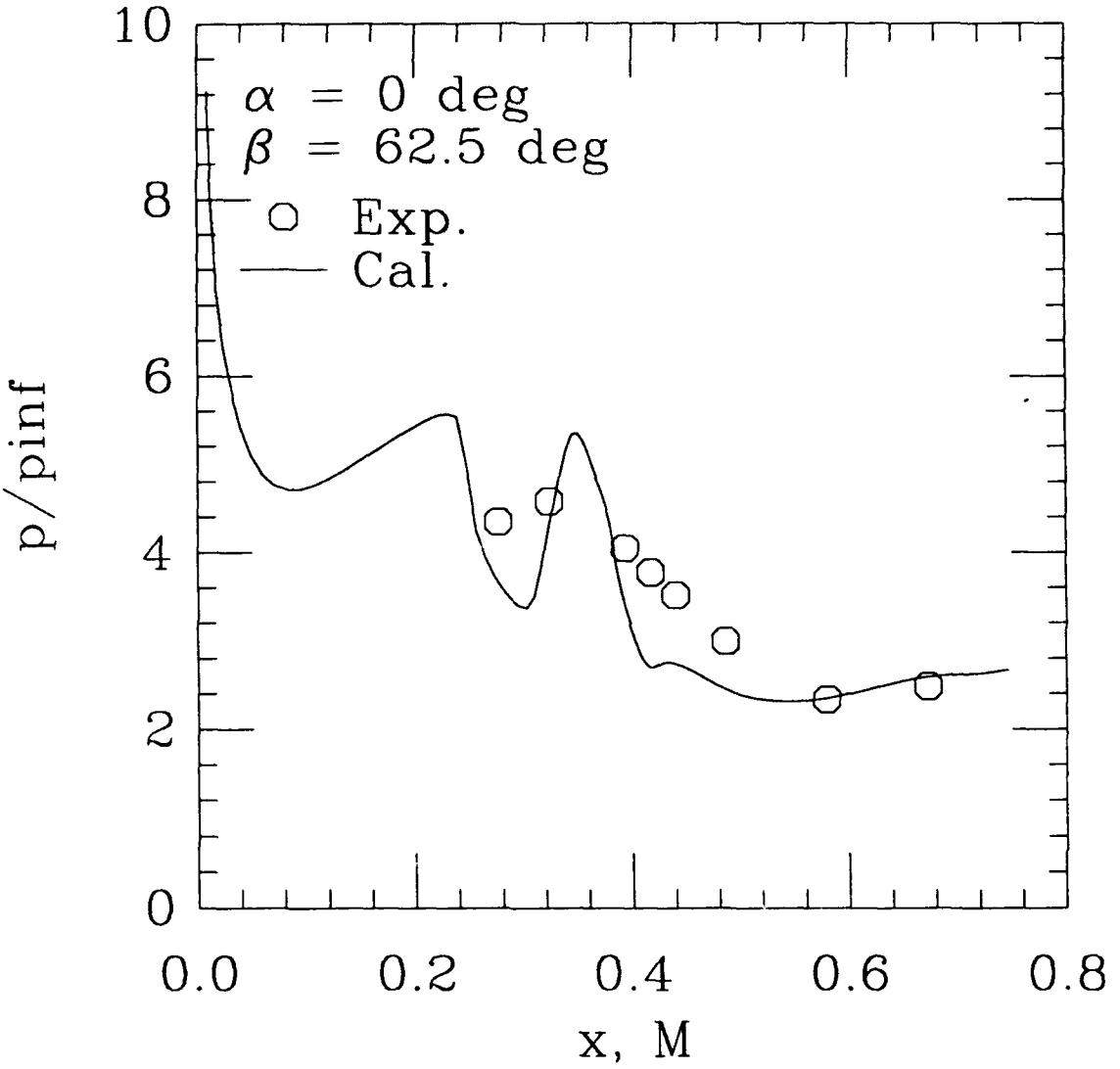

(d)

FIGURE 7. CONTINUED

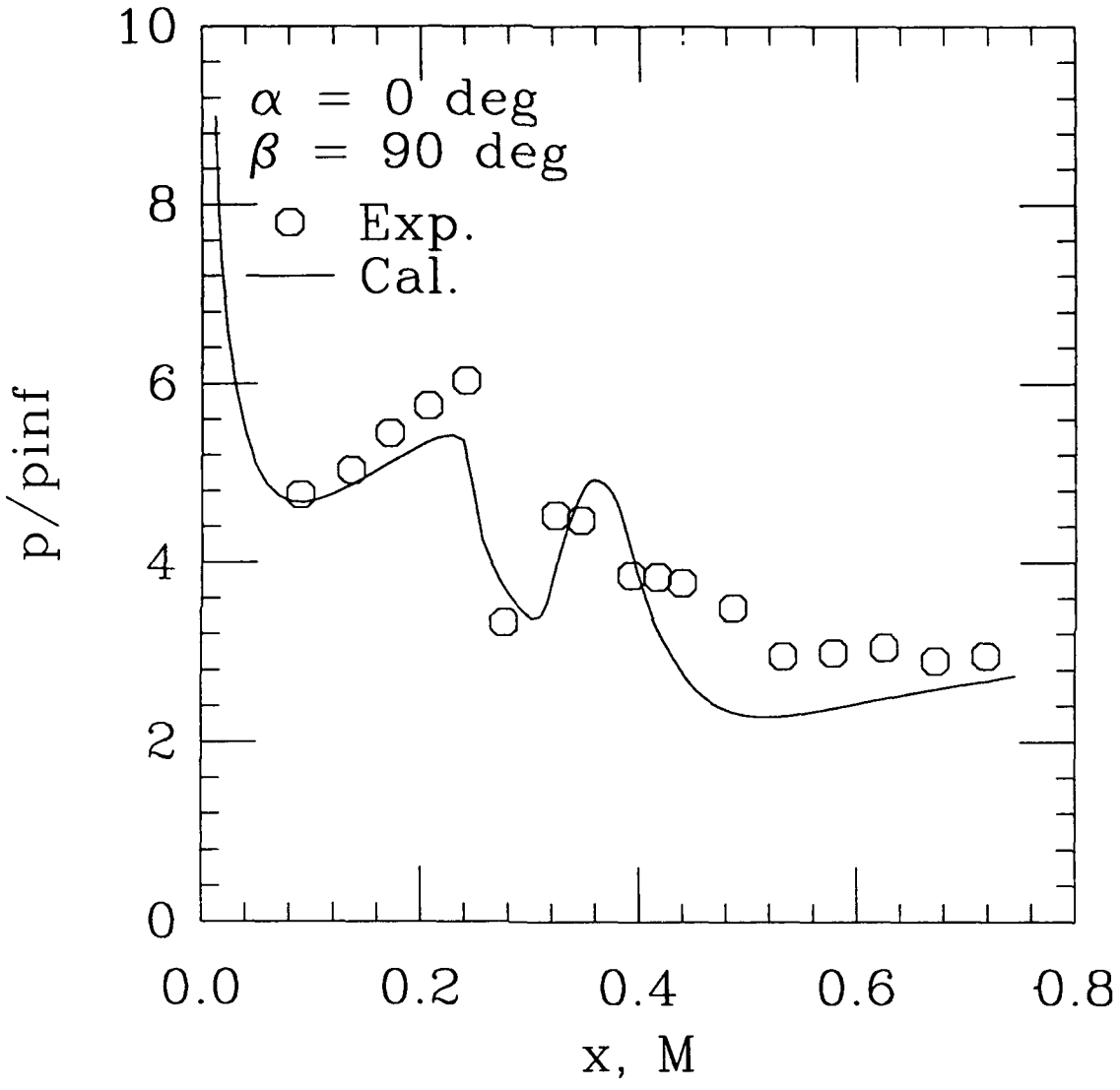

(e)

FIGURE 7. CONTINUED

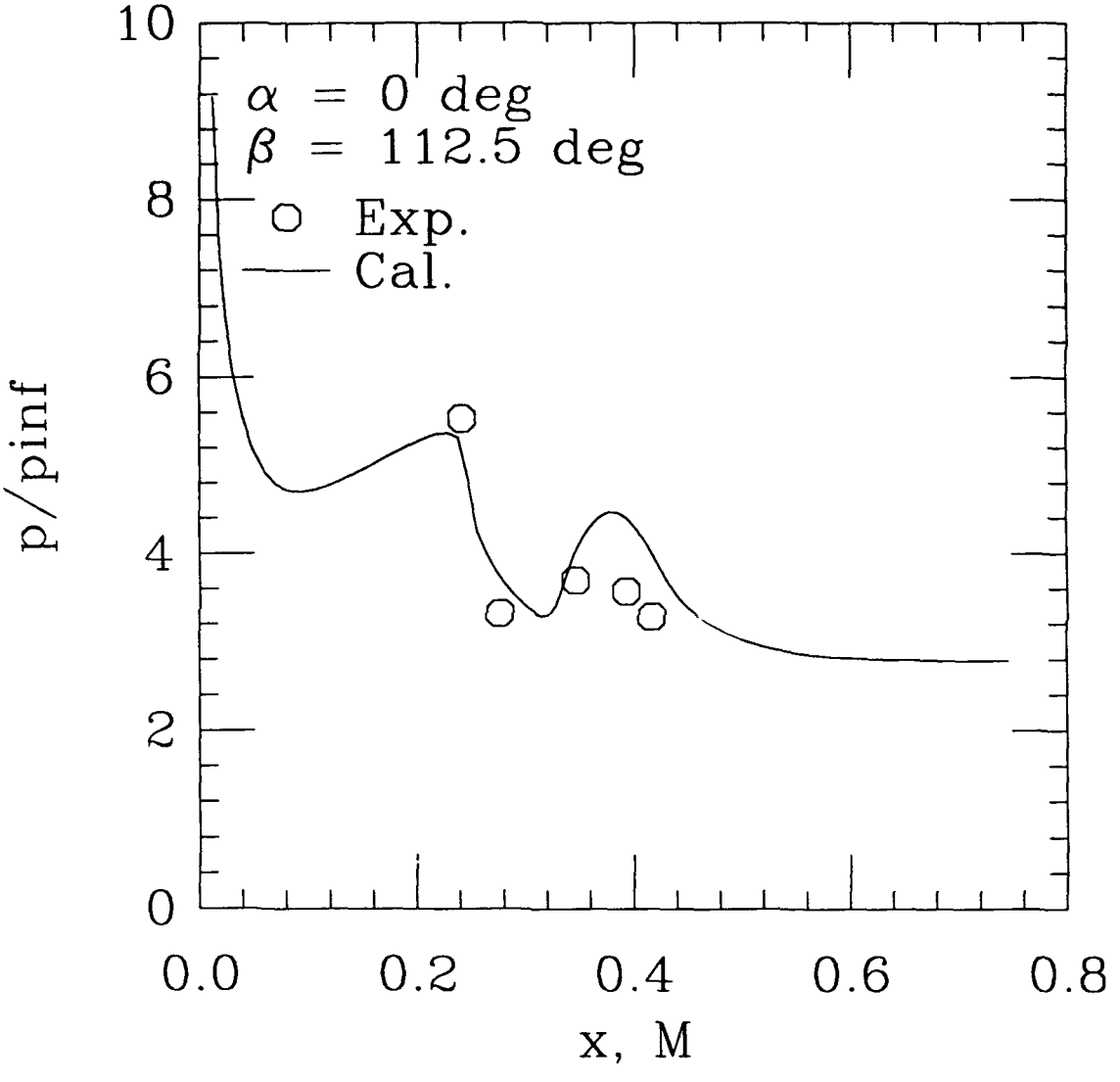

(f)

FIGURE 7. CONTINUED

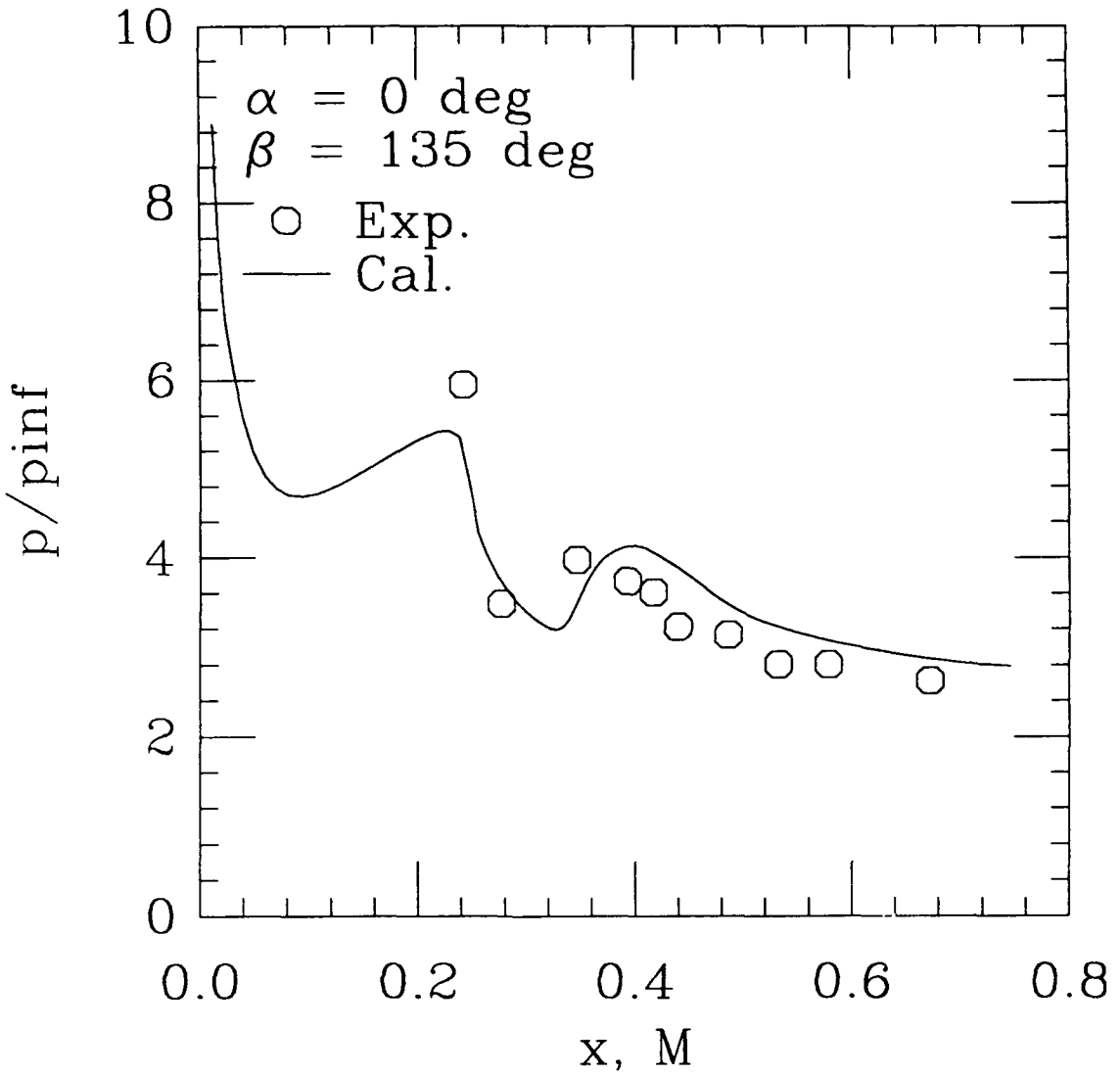

(g)

FIGURE 7. CONTINUED

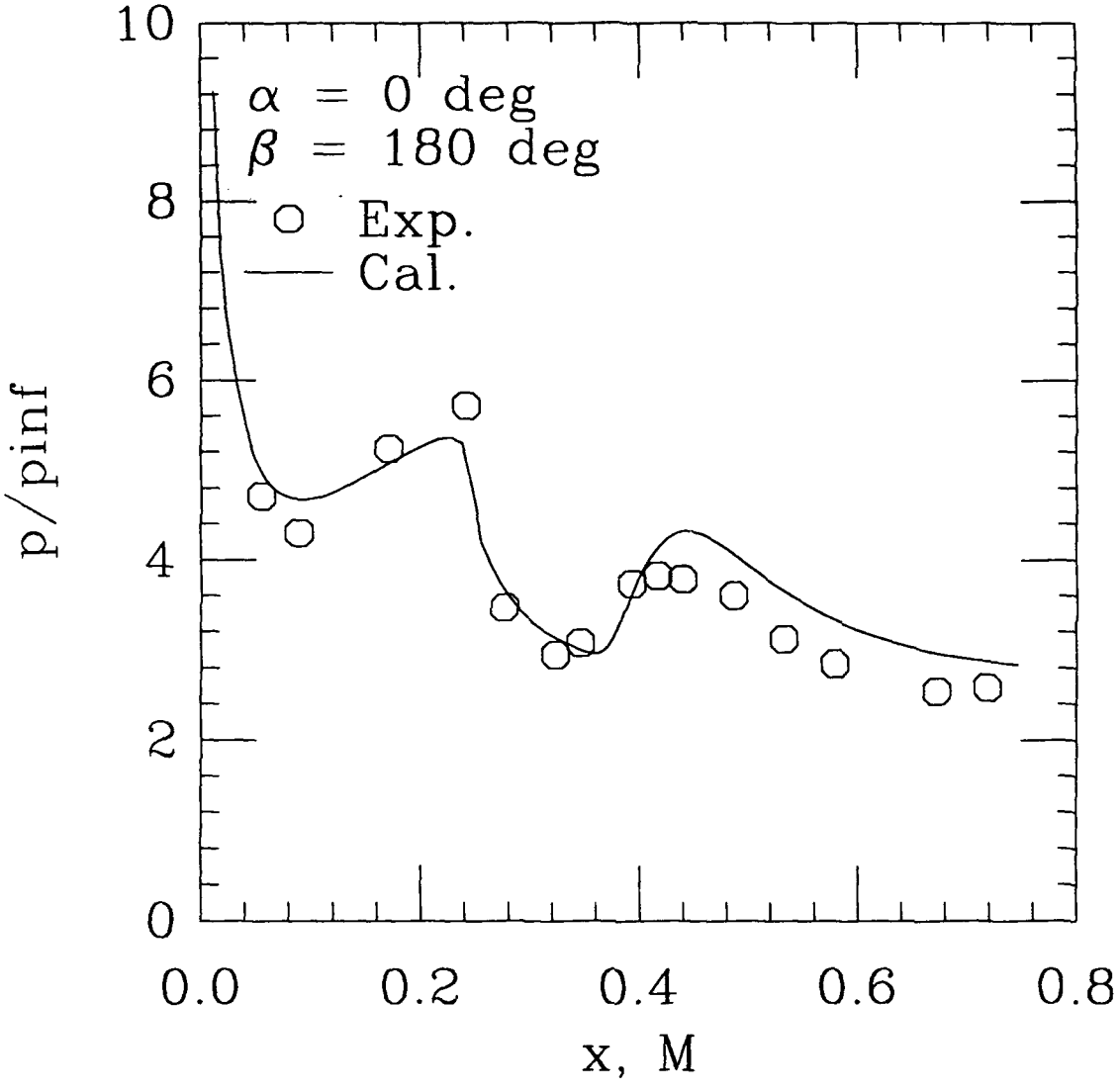

(h)

FIGURE 7. CONCLUDED

FIGURE 8. STREAMLINES FOR THE JET FLOW FIELD
ON THE SYMMETRY PLANE AND THE BODY SURFACE

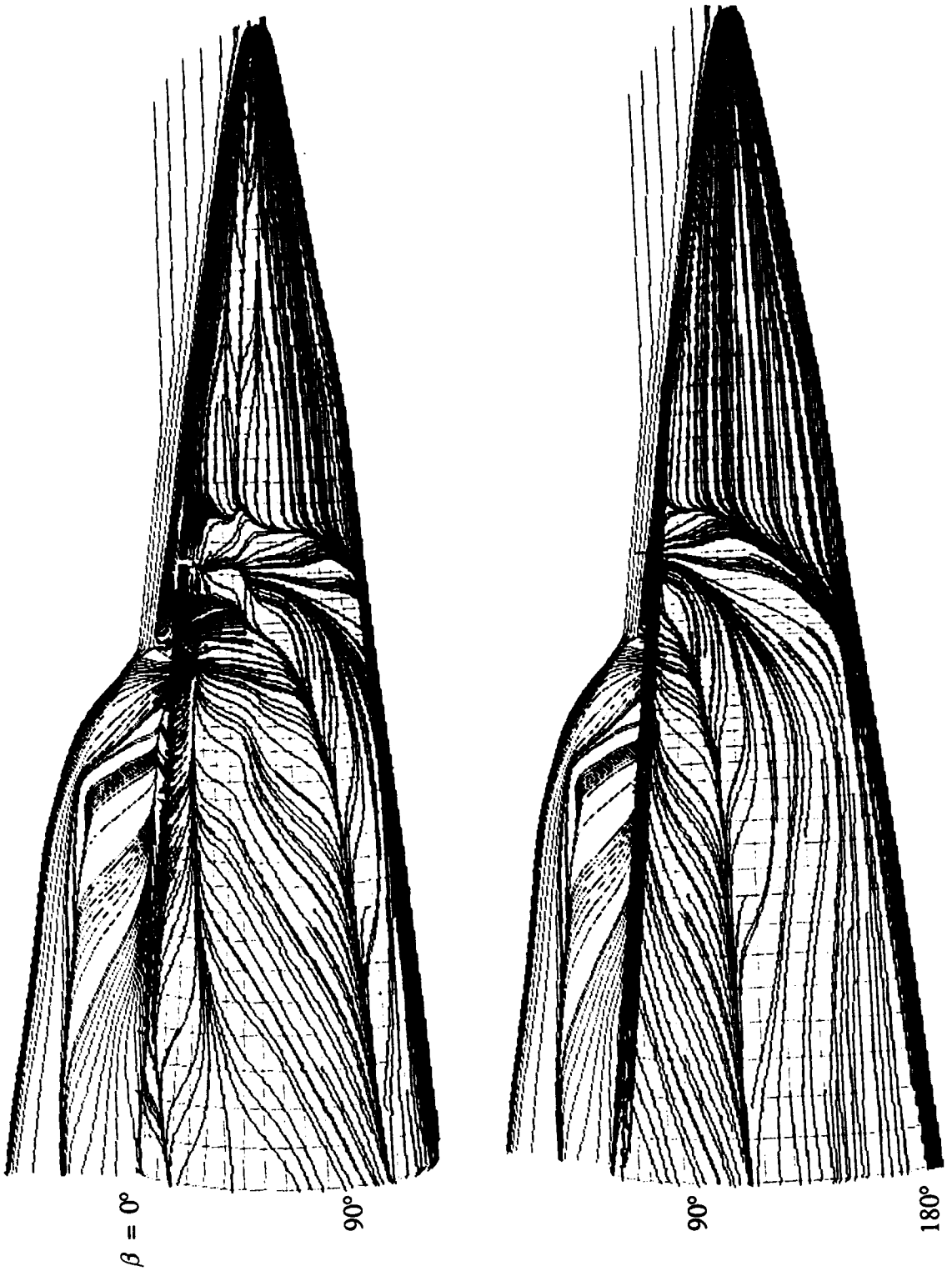

FIGURE 9. DETAILS OF THE THE SURFACE
AND SYMMETRY PLANE STREAMLINES

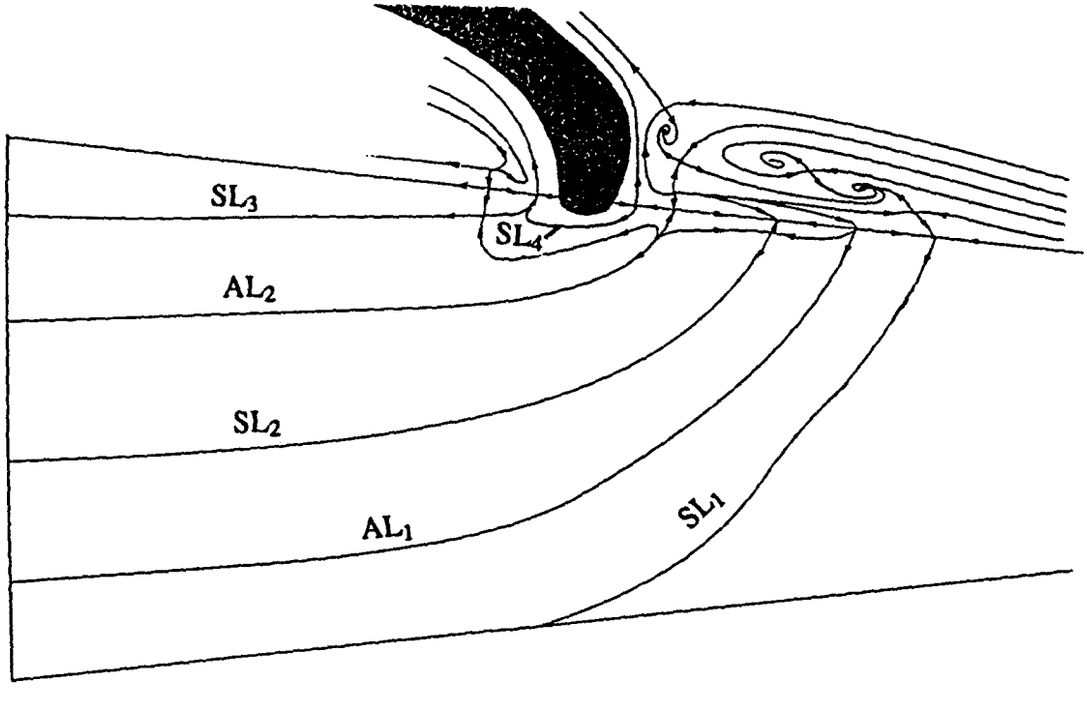

FIGURE 10. SKETCH OF THE STREAMLINE STRUCTURE
ON THE SURFACE AND SYMMETRY PLANE

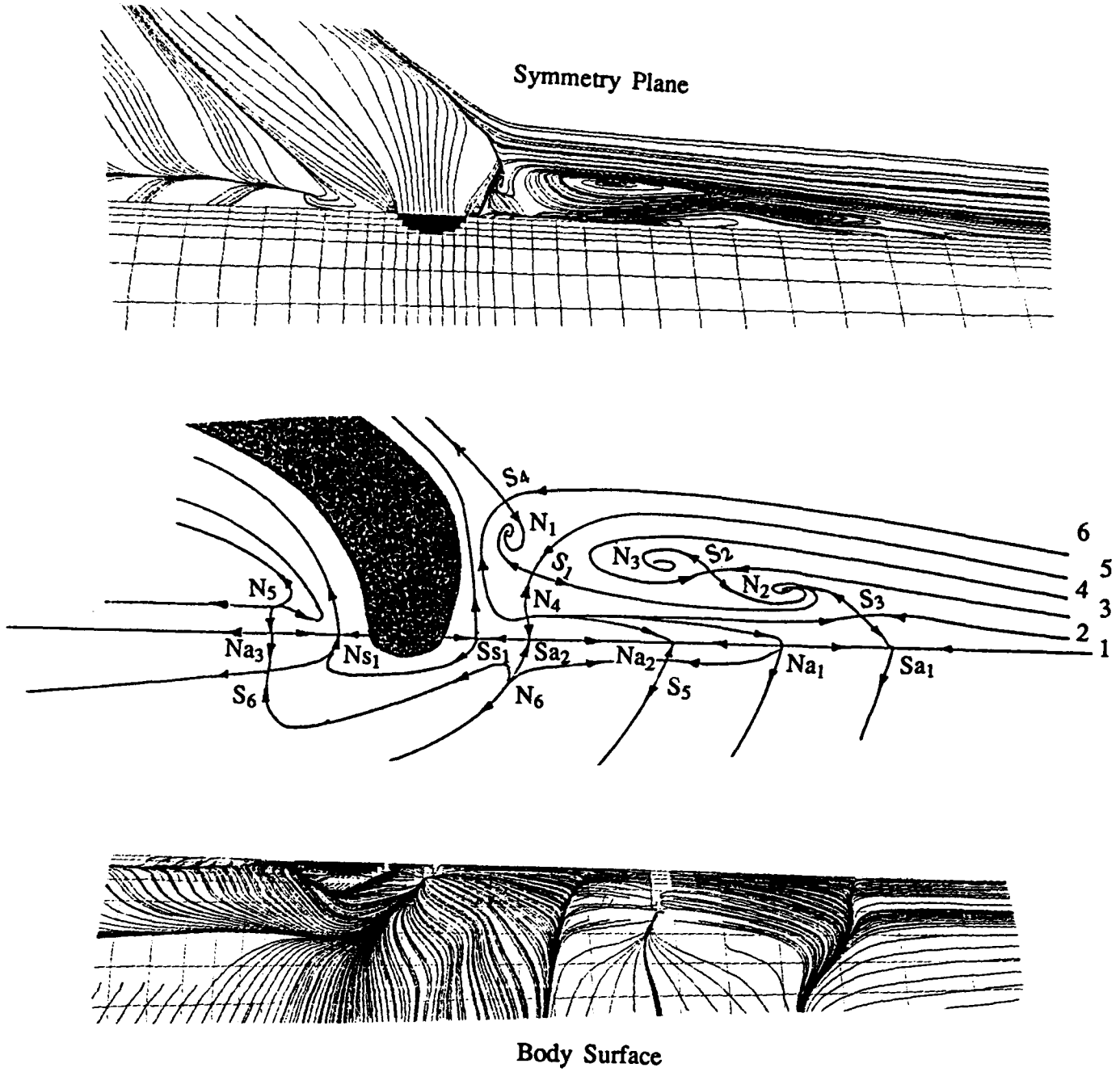

FIGURE 11. DETAIL SKETCH OF FLOW STRUCTURE AND PLOTS OF THE STREAMLINES NEAR THE JET

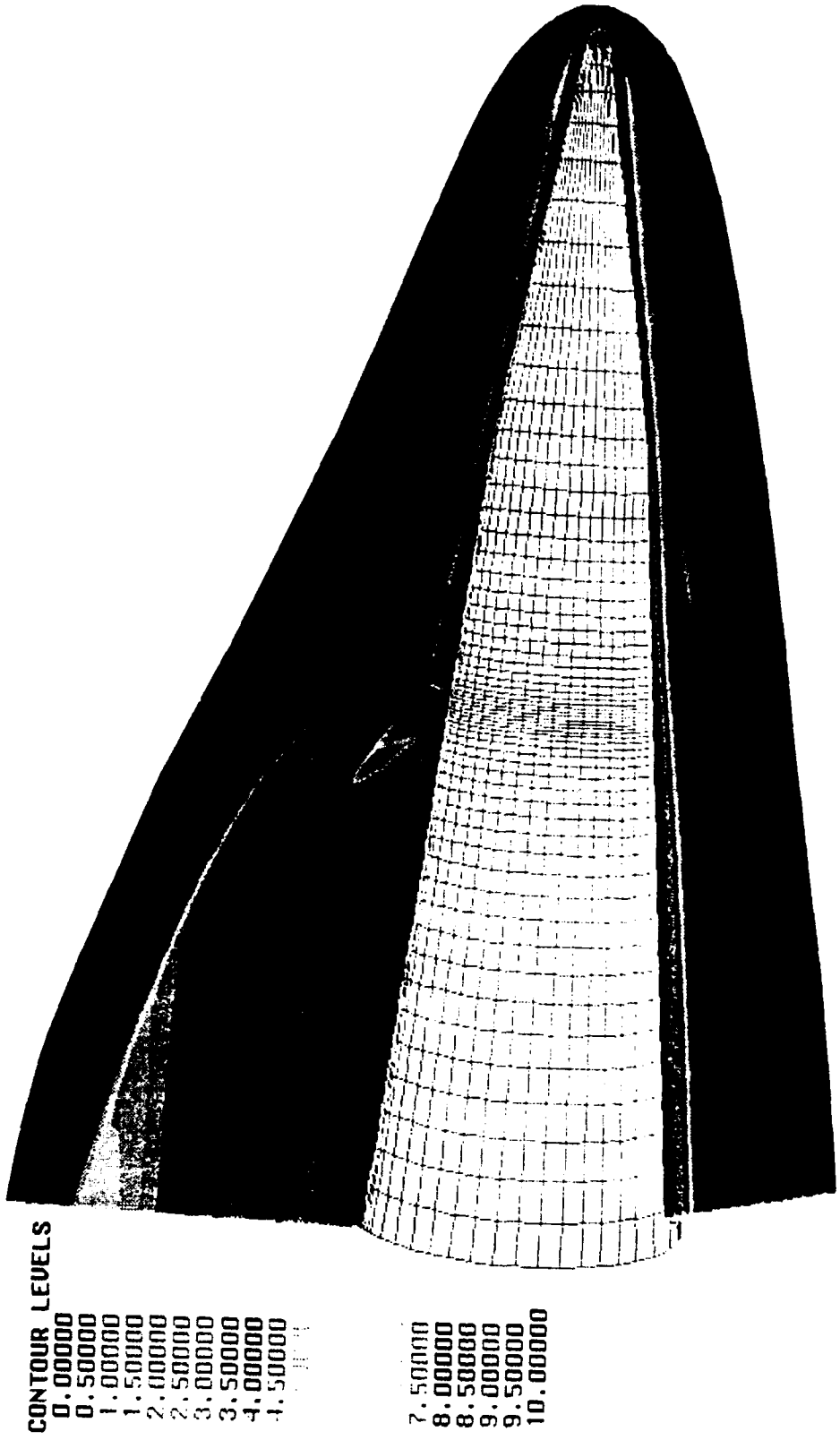

FIGURE 12. MACH CONTOURS ON THE SYMMETRY PLANE

TABLE 1 Three Jet Exit Conditions

Jet	ρ_j/ρ_{inf}	U_j/U_{inf}	p_j/p_{inf}
I	3.215	.477	109.7
II	.461	1.200	4.300
III	2.000	1.200	15.00

CHAPTER 7

REFERENCES

1. Schetz, J. A., "Injection and Mixing in Turbulent Flow" Progress in Astronautics and Aeronautics, Vol. 68, AIAA Publications, 1980.
2. Zukoski, E. E. and Spaid, F. W., "Secondary Injection of Gases into a Supersonic Stream," AIAA J., Vol. 2, October 1964, pp. 1689–96.
3. Prats, B.D., Hill, J.A.F., Metzger, M.A., and Harvey, D.W., "High Altitude Maneuver Control Tests in the NSWC Hypervelocity Wind Tunnel," AIAA Paper 84–0616, March, 1984.
4. Shang, J.S., McMaster, D.L., Scaggs, N., and Buck, M., "Interaction of Jet in Hypersonic Cross Stream," AIAA Paper 87–0055, Jan. 1987, also AIAA J., vol. 27, March 1989, pp. 323,329.
5. McMaster, D.L., Shang, J.S., and Golbitz, W.C., "Supersonic, Transverse Jet from a Rotating Ogive Cylinder in a Hypersonic Flow," AIAA Paper 87–1441, June 1987.
6. Yeneriz, M.A., Davis, J.C., Cooper, G.K., and Harvey, D.W., "Comparison of Calculation and Experiment for a Lateral Jet from a Hypersonic Biconic Vehicle," AIAA Paper 89–2548, July 1989
7. McDonough, J.M. and Catton, I., "Calculation of a Lateral Jet in a Hypersonic Cross-Flow," AIAA Paper 89–2549, July 1989.
8. Chamberlain, R.R., "Calculation of Three Dimensional Jet Interaction Flowfields," AIAA Paper 90–2099.
9. McDonough, J.M., Weatherly, D.C., and Catton, I., "Further Studies of Supersonic Jet Interaction with a Hypersonic Crossflow," AIAA Paper 90–2101, July 1990.
10. Yeneriz, M.A., Davis, J.C., and Harvey, D.W., "Comparison of Calculation and Experiment for a Lateral Jet from a Hypersonic Biconic Vehicle, Part II: Effect of Angle of Attack," AIAA Paper 90–2104, July 1990.
11. Walters, R.W., Slack, D.C., Cinnella, P., Applebaum, M.P., and Frost, C., "A User's Guide to GASP," Virginia Polytechnic Institute and State University, Dept. of Aerospace and Ocean Engineering, Nov 1990.
12. Thomas, J.L., Taylor, S.L., and Anderson, W.K., "Navier-Stokes Computations of Vortical Flows Over Low Aspect Ratio Wings," AIAA paper 87–0207, Jan. 1987.
13. Thomas, J.L., Walters, R.W., Reu, T., Ghaffini, S., Weston R.P., and Duckering, J.M., "Patched Grid Algorithm for Complex Configurations Directed Toward F-18 Aircraft," AIAA Paper 89–0121, Jan. 1989.
14. Roe, P.L., " Approximate Riemann Solvers, Parameter Vectors, and Difference Schemes," J. Comp. Phys., 43, 1981, pp 357–372.

15. Hsieh, T., Wardlaw, A.B. Jr., and Birch, T.J., "Vortical Flows About a Long Ogive-Cylinder at M=3.5 and α=18°," AIAA Paper 91–1808, June 1991.
16. Harvey, D.W., private communication.
17. Lighthill, M.J., "Boundary Layers and Separation," Laminar Boundary Layer, edited by L. Rosenhead, Oxford Uni. Press, Oxford England, UK 1963.
18. Chan, S. C., Rogers, R. P., Edwards, G. L., and Brooks, W. B., "Integrated Jet Interactions and Comparison to Force and Momement Measurements for a Thruster Altitude Controlled Missile," AIAA Paper 93–3522, Aug. 1993.
19. Hung, C.M., Sung, C.H. and Chen C.L., "Computation of Saddle Point of Attachment," AIAA Journal, Vol. 30, No. 6, June 1992, pp1561–1569.

DISTRIBUTION

	Copies
DoD ACTIVITIES (CONUS)	
DEFENSE TECHNICAL INFORMATION CENTER CAMERON STATION ALEXANDRIA VA 22304-6145	12
NON-DoD ACTIVITIES	
ATTN GIFT & EXCHANGE DIV LIBRARY OF CONGRESS WASHINGTON DC 20540	4
CENTER FOR NAVAL ANALYSES 4401 FORD AVE ALEXANDRIA VA 22302-0268	1

	Copies
INTERNAL	
E231	2
E232	3
R44 (T HSIEH)	10
R44 (A WARDLAW)	10

REPORT DOCUMENTATION PAGE

Form Approved OMB No. 0704-0188

1. AGENCY USE ONLY *(Leave blank)*	2. REPORT DATE	3. REPORT TYPE AND DATES COVERED
	8 March 1994	

4. TITLE AND SUBTITLE
Numerical Simulation of Lateral Thrusters om Hypersonic Flow Over a Biconic Body

5. FUNDING NUMBERS

6. AUTHOR(S)
T. Hsieh and A. B. Wardlaw, Jr.

7. PERFORMING ORGANIZATION NAME(S) AND ADDRESS(ES)
Naval Surface Warfare Center
Dahlgren Division, White Oak Detachment
10901 New Hampshire Avenue
Silver Spring, MD 20903-5640

8. PERFORMING ORGANIZATION REPORT NUMBER
NSWCDD/TR-93/138

9. SPONSORING/MONITORING AGENCY NAME(S) AND ADDRESS(ES)

10. SPONSORING/MONITORING AGENCY REPORT NUMBER

11. SUPPLEMENTARY NOTES

12a. DISTRIBUTION/AVAILABILITY STATEMENT
Approved for public release; distribution is unlimited.

12b. DISTRIBUTION CODE

13. ABSTRACT *(Maximum 200 words)*

A Navier-Stokes simulation of lateral thrusters on a biconic body in hypersonic flow is presented. Due to simplifications arising from symmetry, cruciform thrusters were considered first. A grid convergence was conducted to evaluate computational accuracy. This was followed by the computation of three different jet exit conditions and an assessment of the flow field changes produced by each. Of particular concern was the possibility of entrapment of streamlines from the jet in a recirculation region upstream of the jet. The final case considered was a single jet thrusting from a biconic body at zero incidence at M = 9.7. These results were compared to experimental surface pressures. A description of the complicated interacting flow fields featuring multiple separation and attachment lines/regions is also presented

14. SUBJECT TERMS
Biconic Body Hypersonic Flow

15. NUMBER OF PAGES
42

16. PRICE CODE

17. SECURITY CLASSIFICATION OF REPORT	18. SECURITY CLASSIFICATION OF THIS PAGE	19. SECURITY CLASSIFICATION OF ABSTRACT	20. LIMITATION OF ABSTRACT
UNCLASSIFIED	UNCLASSIFIED	UNCLASSIFIED	SAR